Towards 3D analysis of pulp fibre networks at the fibre and bond levels

C. Marulier, P.J.J. Dumont, L. Orgéas, D. Caillerie, S. Rolland du Roscoat

KEYWORDS: Lignocellulosic fibre networks, Computerised X-ray synchrotron microtomography, Wet pressing, Microstructural properties, Mechanical properties, Fibre free segment length, Fibre cross section morphology and inclination, Bond area surface distribution.

SUMMARY: By using X-ray synchrotron microtomography imaging, this work aims at proposing a method to get 3D information on paper fibrous microstructures. Such technique is useful to better understand the links between the manufacturing conditions, the resulting microstructural and mechanical properties of the paper fibrous networks, together with the morphology of fibres and fibre-fibre bonds. Its usefulness is illustrated for the 3D analysis of model papers being produced by changing the wet pressing conditions. It is demonstrated that the image analysis allows the changes of parameters describing, for example, the fibre cross section shape and inclination, the bond area surfaces, the distance between bonds to be followed with respect to the processing conditions for a large set of fibres and bonds. The distributions of properties that can be drawn from this experimental analysis will allow mechanical or physical discrete modelling approaches for papers to be enriched.

ADDRESSES OF THE AUTHORS: C. Marulier, P.J.J. Dumont (pierre.dumont@grenoble-inp.fr), Grenoble INP / CNRS, Laboratoire de Génie des Procédés Papetiers (LGP2), 461 rue de la Papeterie, BP 65, 38402 Saint-Martin-d'Hères cedex, France.
L. Orgéas, D. Caillerie, S. Rolland du Roscoat, Université de Grenoble (Grenoble INP - UJF) / CNRS, Laboratoire Sols-Solides-Structures-Risques (3SR Lab), BP 53, 38041 Grenoble cedex 9, France.
S. Rolland du Roscoat, European Synchrotron Radiation Facility (ESRF), ID 19 Topography and Microtomography Group, 38043 Grenoble cedex, France.
Corresponding author: P.J.J. Dumont

Papermaking conditions (forming, pressing and drying) govern the architecture of the resulting pulp fibre networks, the complex morphology (Sampson 2009) and the states of residual stresses in fibres and fibre-fibre bonds (Uesaka et al. 1991).

Recently, several microscopic techniques (optical microscopy, Scanning Electron Microscopy (SEM), Environmental Scanning Electron Microscopy (ESEM), Transmission Electron Microscopy (TEM), Fluorescence Resonance Energy Transfer (FRET) microscopy, confocal laser scanning microscopy) have been used to estimate some important microstructure descriptors such as the fibre-fibre bond surface (Nanko, Ohsawa 1989; Batchelor, Kibblewhite 2006a; Thomson et al. 2008a; Thomson et al. 2008b; Kappel et al. 2009; Kappel 2010a; Kappel et al. 2010b), the fibre width, thickness or wall properties (Nanko, Ohsawa 1989; He et al. 2004; Chinga-Carrasco et al. 2010; Wiltsche et al. 2011), the number of bonds between fibres (Batchelor et al. 2006b). A first group of studies focuses on the analysis of single fibre-fibre bonds prepared in conditions that were far from the usual paper processing conditions (Thomson et al. 2007; Torgnysdotter et al. 2007; Thomson et al. 2008a; Thomson et al. 2008b; Kappel et al. 2009; Kappel et al. 2010a; Kappel et al. 2010b). A second group tried to extract such microstructural descriptors directly from the image analysis of fibrous networks processed following more classical papermaking conditions (He et al. 2003a; He et al. 2003b; He et al. 2004). These approaches are very interesting because they can potentially highlight the influence of the network structure on the fibres and fibre-fibre bonds during papermaking unit operations. However, these methods are destructive (as the tested specimens can only be used once) and may be time consuming. They also present difficulties to extract 3D information because the data are extracted from 2D views or 2D projections or very low depth of field 3D images. Lastly, if many descriptors were measured in these studies, the description of the fibre-fibre bonds should be improved.

To overcome this problem, X-ray microtomography appears as a very powerful microstructure analysis method (Baruchel et al. 2000; Rolland du Roscoat et al. 2005; Le et al. 2008; Délisée et al. 2009; Salvo et al. 2010; Malmberg et al. 2011; Orgéas et al. 2012; Guiraud et al. 2012). Huge progress in imaging paper-like materials have been recently made as exemplified by the progression that can be observed from the pioneering work of Samuelsen et al. (1999), Samuelsen et al. (2001) and Antoine et al. (2002) up to the most recent studies (Rolland du Roscoat et al. 2005; Holmstad et al. 2006; Rolland du Roscoat et al. 2007; Rolland du Roscoat et al. 2008; Axelsson, Svensson 2010; Chinga-Carrasco 2011; Viguié et al. 2011). Microtomography images can be used to perform relevant structural analysis so as to determine the porous properties of such fibrous materials (Rolland du Roscoat et al. 2007), the ink-paper or liquid interaction (Vernhes et al. 2007; Koivu et al. 2010), or to support the determination of physical paper parameters such as those related to their permeability (Koivu et al. 2009), thermal (Rolland du Roscoat et al. 2008), or hygroexpansion properties (Viguié et al. 2011) when the acquired images are coupled to numerical simulation softwares and/or digital image correlation techniques.

However, to date, the microstructure analyses have mainly focused on global fibrous network properties (porosity, specific surface, etc.). The analysis of the morphology properties of individual components such as the fibre or bond geometries has not yet been undertaken using such types of images. When considering network or particle models (Jayaraman, Kortschot 1998; Heyden, Gustafsson 2001; Strömbro, Gudmundson 2008; Åslund,

Isaksson 2011; Liu et al. 2011) to predict the physical, and especially the mechanical, properties of pulp fibre networks, information about the morphology or the physical properties of fibres and bonds is paramount. But it remains extremely difficult to perform relevant multiscale analyses because these properties are not easily accessible ex situ and are obviously much more difficult to obtain in situ. Therefore, this work primarily aims at proposing an analysis method to get accurate and 3D information on the paper fibrous networks for different manufacturing conditions. This work also aims at interpreting the microstructure changes regarding the process and to briefly relate the latter to the changes of the paper mechanical properties. Such method is based on a fine analysis of images acquired by X-ray synchrotron microtomography of model papers fabricated using classified pulp fibres and varying pressing conditions.

In a first section, the pulp fibres and the processing conditions to obtain model papers are given. The X-ray synchrotron microtomography imaging technique and the image analysis treatments to improve the image quality are also explained. Finally, the performed mechanical tests are described. In a second section, the way the fibre network microstructure parameters are determined at the network and fibre or fibre-fibre bond scales are detailed. The influence of pressing conditions at the macroscopic and lower relevant scales are then presented. Finally, the relevance and the novelty of the obtained microstructural observations is discussed by comparison with data obtained in the literature for similar types of analysis utilising classical observation techniques. Furthermore, the interest of the observed tendencies for mechanical discrete models of pulp fibre networks is briefly discussed.

Materials and experimental procedure

Fibres

The raw material used for the model papers was a bleached softwood pulp from maritime pine. No beating operation was carried out to avoid damage phenomena such as cutting effects or fibrillation of the single fibre structures. In its initial state, this pulp contained a significant amount of fibres longer than 2 mm: see *Fig 1(a)*. Further, a screening operation (Bauer Mac Nett device) was performed to remove particles smaller than 0.5 mm. Such operation was performed to obtain fibrous networks where the fibrous elements have "simple" geometries and calibrated sizes. The length of the pulp fibres given in *Fig 1(b)* was measured using the MOrFI device (Techpap, Grenoble, France).

Model papers processing

Paper handsheets having a targeted basis weight of 40 g m^{-2} and an in-plane isotropic structure were produced using a Rapid Köthen former (Karl Frank GMBH, Weinheim, Germany). The random orientation of the fibres in the midplane of the sheet was controlled after the formation operation: see *Fig 1(c)* where a typical fibre orientation distribution is depicted for those materials where 0.5% of the pulp fibres were red dyed to perform this measurement. The wet handsheets were then pressed between blotters for 3 min using a press equipped with two parallel plates that could control the normal applied packing stress σ_0. This latter was respectively set to 0.10 MPa, 0.51 MPa and 0.91 MPa so as to adjust the density of the produced papers (Alexander, Marton 1968).

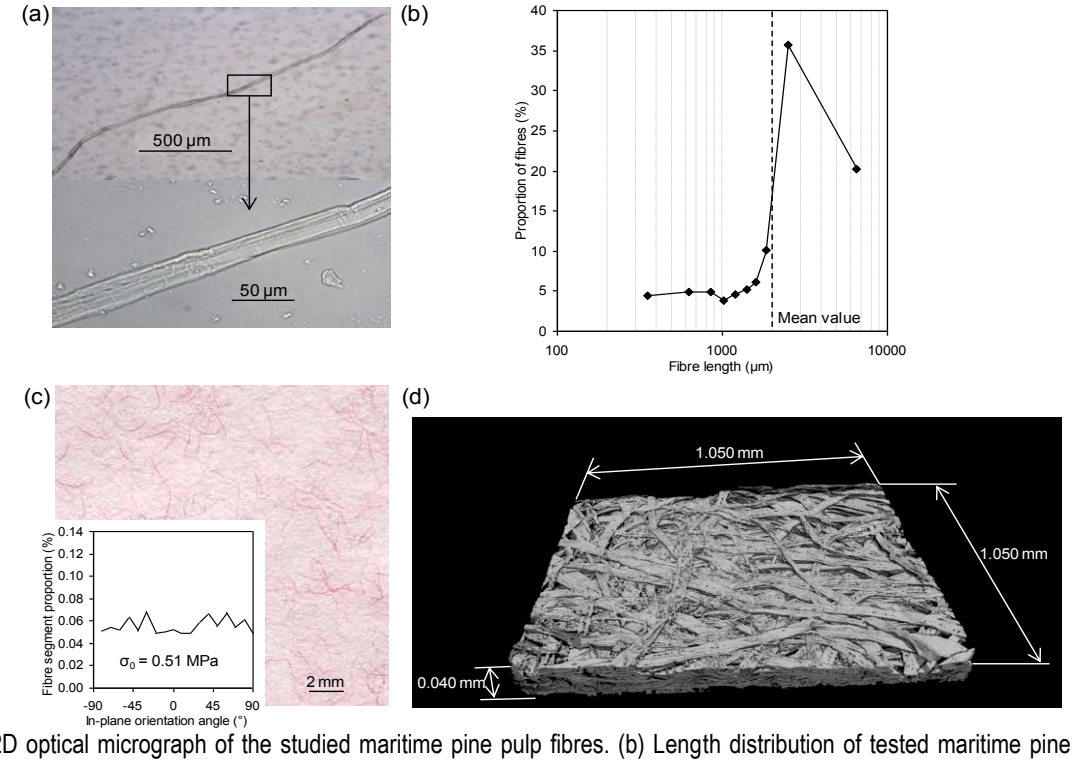

Fig 1. (a) 2D optical micrograph of the studied maritime pine pulp fibres. (b) Length distribution of tested maritime pine pulp fibres after the screening operation. (c) Top view of a model paper (σ_0 = 0.51 MPa, some of the fibres were previously dyed in order to assess the spatial distribution of fibres together with their 2D orientation, see the graph onto the picture). (d) 3D reconstruction obtained by X-ray microtomography (ESRF, beamline ID 19) of an isotropic paper wet pressed at σ_0 = 0.51 MPa.

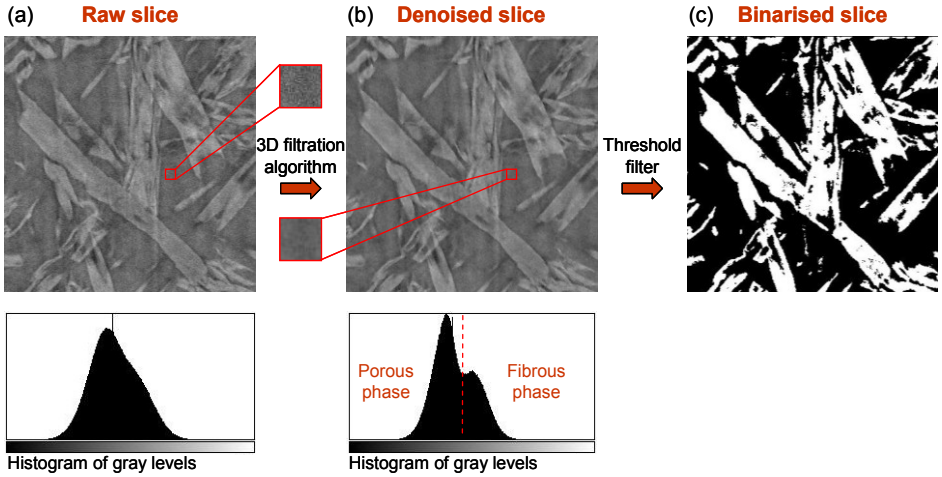

Fig 2. Method used to extract 3D segmented images of the fibrous microstructures from the 3D grayscale images acquired with the X-ay microtomograph.

After pressing, the handsheets were finally dried with in-plane constrained conditions in the Rapid Köthen machine drying system for 6 min at 85°C. It was checked that the handsheets did not exhibit after drying any in-plane shrinkage and any out-of-plane deformations such as curl or cockles. Such constrained drying conditions are known to induce residual stresses inside the free fibre segments located between two bonds, but also in the fibre-fibre bonds (Uesaka et al. 1991).

Microstructure imaging

X-ray microtomography was performed at the European Synchrotron Radiation Facility (ESRF, ID19 beamline, Grenoble, France) to perform 3D characterization of the fibrous microstructures of the produced papers. Fast scans (overall scanning time ≈ 5 min) of small paper specimens of dimensions ≈ 1.4 mm × 1.4 mm × t mm, where t is the thickness of the paper, extracted from the produced sheets were achieved. The scans consisted of acquiring 1500 X-ray 2D radiographs onto a CCD detector (field of view 2048 × 2048 pixels) obtained from the incremental rotation of the imaged sample with respect to the synchrotron X-ray monochromatic source (overall rotation = 180°, X-ray energy = 17.6 ± 0.9 keV). The combination of the CDD detector and the optics allowed a pixel size of 0.7 µm × 0.7 µm to be obtained. Then, the 2D radiographs were filtered to remove ring artefacts. This new set of radiographs becomes the input of the filter back projection algorithm that provides the 3D data sets, i.e. a cylindrical volume of $\pi d^2 t/4$ (d = 1.4 mm). We therefore obtained 3D maps of the X-ray absorption coefficient within each scanned specimen. A reconstructed image of the cross section of a typical specimen is given in *Fig 2(a)*. To obtain quantitative structural parameters, the two main phases of the paper specimens, i.e. the pore phase and the solid fibrous phase were segmented. Due to the rather poor absorption contrast between these two phases, a special procedure was required for that purpose. A preliminary step consisted of denoising the data to enhance the segmentation (see in *Fig 2(b)* the denoised image of the previously displayed specimen cross section). The used denoising algorithm is based on a nonlinear anisotropic diffusion filter (Perona, Malik 1990; Rolland du Roscoat et al. 2005). Then the segmentation lay on a seeded region growing method based on voxel aggregation (Rolland du Roscoat et al. 2005). *Fig 2(c)* shows the resulting segmented cross section. This process was performed using volumes of 1.05 mm × 1.05 mm × t mm, corresponding to parallelepiped contained in the reconstructed cylindrical volume. As an example, *Fig 1(d)* shows a 3D example of a reconstructed and segmented fibrous networks wet pressed at σ_0 = 0.51 MPa.

Basic structural and mechanical properties

Basic structural properties (thickness, basis weight, porosity) were then measured for each handsheet after processing and storage in environmentally controlled rooms (T=23°C and 50% RH) to estimate the paper apparent density ρ_{app}. The apparent porosity Φ_{app} of papers were also estimated from ρ_{app} and from the density of pure cellulose $\rho_{cellulose}$ taken equal to 1500 kg m^{-3} (Salmén, Fellers 1989), and considering that fibres were only composed of cellulose.

$$\Phi_{app} = 1 - \frac{\rho_{app}}{\rho_{cellulose}}. \qquad [1]$$

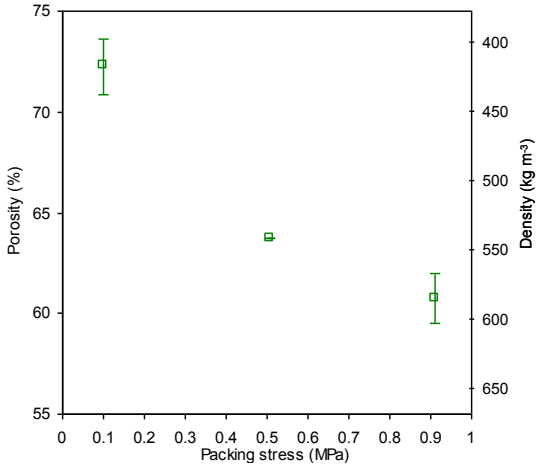

Fig 3. Porosity Φ_{app} and corresponding density ρ_{app} of model papers (HR = 50%) as a function of the packing stress. Porosity data are averaged over five test results for each paper type. The minimum and maximum values are used to show the scatter of the measurements.

Table 1. Porosity of model papers (HR = 50%) with respect to the wet pressing stresses determined using a standard determination technique Φ_{app} and direct measurements on X-ray imaged specimens Φ_X.

Packing stress σ_0 (MPa)	0.10	0.51	0.91
Average apparent porosity Φ_{app} (%)	73	64	61
X-ray measured porosity Φ_X (%)	86	73	-

The porosity of model papers decreases from 73% to 61% as the packing stress increases from 0.10 MPa to 0.91 MPa (*Fig 3*) during wet pressing: see *Fig 3* where the corresponding apparent densities are also indicated. The decrease of porosity when changing the packing stress from 0.10 MPa to 0.51 MPa is comparatively higher (decrease of 12%) than when increasing the packing stress from 0.51 MPa to 0.91 (change of 4%). Such limited consolidation which tends to stabilise at high packing stress is classically observed during wet pressing of papers (Luner et al. 1961; Alexander, Marton 1968).

Note that the porosity of the model papers was also calculated using the segmented X-ray microtomography volumes. In that case, the porosity Φ_X of the scanned specimens was estimated as the ratio between the sum of the black voxels (i.e. the volume occupied by the pores) and the sum of all voxels (i.e. the volume of the imaged specimens). Corresponding results are gathered in *Table 1* together with those measured with the standard method. Φ_{app} and Φ_X follow the same trends, i.e. a decrease with the packing stress σ_0. Nevertheless, for the same value of σ_0, Φ_{app} and Φ_X differ so that $\Phi_X > \Phi_{app}$. Such a mismatch can be explained by the differences in both measurement techniques: the standard method used to estimate Φ_{app} led to slightly pack paper specimens when measuring their thickness, whereas this was not the case when using the X-ray images of the paper specimens. Please note that in the following, the indicated porosities (or the corresponding densities) are those measured using the standard method. The mechanical properties of model papers were studied by using a commercial horizontal tensile testing device (Lorentzen & Wettre No. 162, tensile tester) that was installed in an air conditioned room (T = 23°C, RH = 50%). To achieve the tests, paper strips having a gauge length of 100 mm (i.e. length between jaws), and a gauge width of 15 mm were cut from the sheets. The Young's modulus E and the breaking stress σ_u could thus be obtained for each specimen. As shown in *Fig 4*, increasing the density of the sample has a predominant effect on increasing both the Young's modulus and the breaking stress of tested model papers. The Young's modulus, resp. the breaking stress, increases from 1050 MPa to 2900 MPa, resp. from 4.7 MPa to 15.1 MPa, as the apparent density increases from 440 kg m^{-3} to 595 kg m^{-3}. Furthermore, there exists a critical (or threshold) density that can be extrapolated equal to 350-400 kg m^{-3} following linear fits of both data shown in the two previous graphs. At this density value, fibres would not create an interconnected fibrous network and therefore the Young's modulus and the breaking stress would be equal to zero.

Geometry of fibres and fibre-fibre bonds

To get quantitative data on the fibrous microstructures, i.e. the fibrous and fibre bond geometries, additional image analysis operations were achieved directly from the binarised images using the software ImageJ ("Pointpicker" plugin). To get such information at the microscopic scale using image analysis standard and automatic algorithms would be very difficult because of the complexity of the studied microstructures. Then, similarly to some previous studies (Le et al. 2008; Latil et al. 2011; Guiraud et al. 2012), a manual approach using binarised images was adopted. The operations are briefly described below and summarised in *Fig 5*. They were performed on two scanned volumes pressed at 0.10 MPa and 0.51 MPa.

• *Characterisation of the fibre centrelines* - Determining the centreline of a considered fibre in the microtomography images was carried out by manually picking the centres of mass of several sections of this fibre parallel to the ($\mathbf{e}_1$, $\mathbf{e}_3$) or ($\mathbf{e}_2$, $\mathbf{e}_3$) planes of the microtomography image frame within bond zones (one picked point per fibre per bond zone) as shown in *Fig 5(a)*. Such points belonging to the centrelines were chosen so that the extremities of the vectors **AB** or **CD** represented in *Fig 5(a)* corresponded to the widest projected dimensions of the bond on the unit vectors $\mathbf{e}_1$ and $\mathbf{e}_2$ of the microtomography frame, respectively. From two picked points on the centreline of the considered fibre *i*, a local unit tangent vector $\mathbf{p}_i$ was defined as illustrated in *Fig 5(a)*.

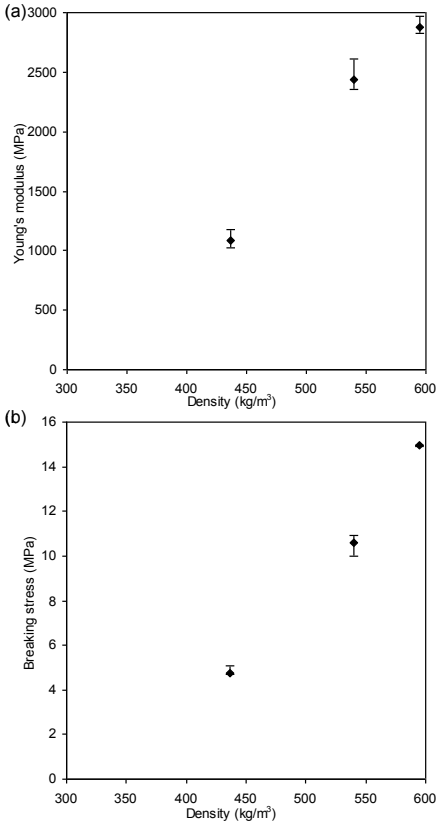

Fig 4. (a) Young's modulus and (b) breaking stress of model papers (HR = 50%) as a function of the apparent density of model isotropic papers. Mechanical data are averaged over five test results for each paper type. The minimum and maximum values are used to show the scatter of the measurements.

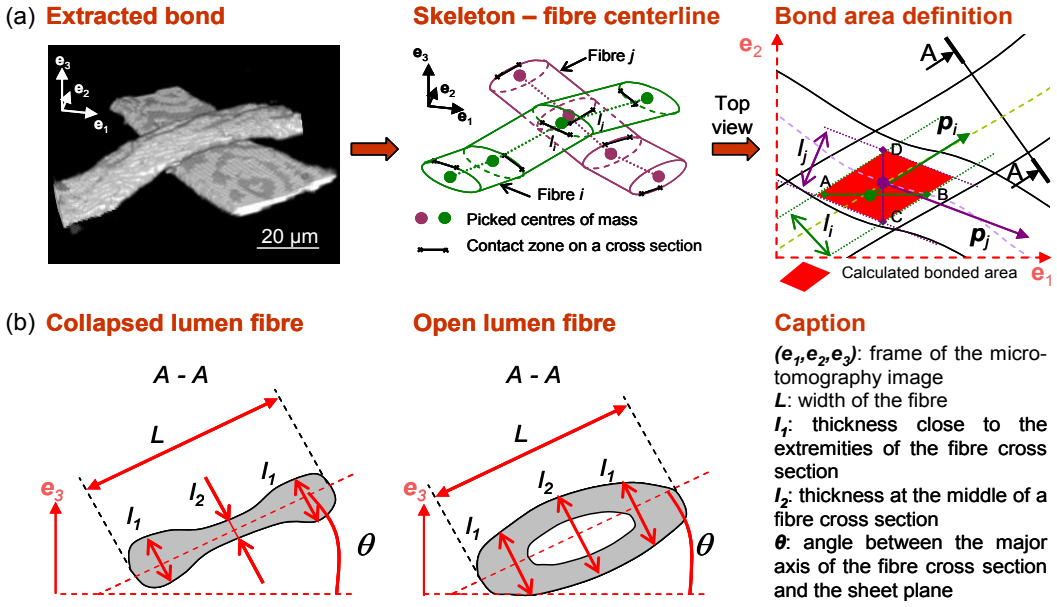

Fig 5. (a) 3D micrograph of a fibre-fibre bond between two contacting fibres extracted from a X-ray microtomography image of a model paper. From such image, the fibre centrelines were determined and the bond surface was calculated. (b) Schematic view of a fibre cross section having a collapsed or an open lumen and principle of determination of the fibre cross section dimensions and of their inclination angle θ.

• *Characterisation of the fibre cross section morphology* – To get estimates of the morphology of the fibre cross sections, the coordinates of some particular points belonging to the cross sections of the considered fibre were measured in order to obtain their principal dimensions: their width L and their thicknesses l_1 and l_2 displayed in *Fig 5(b)*. Two kinds of thicknesses were distinguished as exemplified in *Fig 5(b)*: l_2 was measured in the middle of the fibre cross section, whereas l_1 was measured close to the extremities of the fibre cross section. More precisely, l_1 was measured at a distance roughly equal to $L/6$ from the extremities if the lumen of the fibre was open in the investigated cross section, whereas it corresponded to the maximum thickness of the fibre cross section if the fibre lumen was collapsed as shown in *Fig 5(b)*. This enabled to get the maximum thickness of the section whatever its shape.

Furthermore, as shown in *Fig 5(b)*, the major axes of the cross section of the considered fibre was not necessarily lying within the ($\mathbf{e}_1$, $\mathbf{e}_2$) plane of the microtomography frame. To estimate the inclination of each investigated fibre cross section, the angle θ between the major axis cross section of the fibre and the plane ($\mathbf{e}_1$, $\mathbf{e}_2$), see *Fig 5(b)*, was thus measured. This inclination angle is similar to the so-called "twist" angle in He et al. (2003b).

To obtain statistical representative distributions of those parameters, at least 120 measurements of each of them were performed within a scanned volume. All the fibres contained in several sub-volumes were characterized. Such procedure was followed to avoid analysing fibres having a prominent geometry. Doing so, the shapes of the corresponding distribution functions were shown to become stable for such numbers of measurements. The interval size for plotting frequency distributions is set to 5 µm for L, to 1 µm for l_1 and l_2, and for 5° for θ.

• *Characterisation of bonds* – The various shapes of the cross sections (open or closed lumen) prevented the use of an automatic detection as it has been done by Malmberg et al. (2011). By following the centreline of the considered fibre of the model paper network, it was further possible to detect the positions of its bonds with its neighbouring fibres. The centres of the bonds were determined by the curvilinear abscissae s_i measured along the fibre centreline. Following this procedure, it was possible to obtain the distance Δs between the centres of two consecutive bonds i and $i + 1$ along the fibre (this parameter is also called the free fibre length by He et al. (2004):

$$\Delta s = s_{i+1} - s_i. \qquad [2]$$

The general aspect of the major part of bonds is represented in *Fig 5(a)*. As the fibres were quite flat, the bond area surface S between two contacting fibres i and j could be roughly estimated as equivalent to that of a parallelogram (see the right scheme in *Fig 5(a)*). In most cases, the dimensions of the bonds are not as large as the contacting fibre widths. Therefore, to get a good estimate of the bond area surface, the widths l_i and l_j of the bonds first have to be calculated: see *Fig 5(a)*. Nonetheless, determining directly l_i and l_j from a microtomography image is not easy as any rotation of the image that could allow a direct visualization of the cross section of each fibre in the vicinity of a bond could induce a decrease of its resolution. Therefore, the adopted measurement technique did not require the studied images to be rotated. It was preferably chosen to visually pick the extremities of the vectors **AB** or **CD** represented in *Fig 5(a)* which respectively correspond to the widest projected dimensions of the bond on the unit vectors $\mathbf{e}_1$ and $\mathbf{e}_2$ of the microtomography frame. Knowing these vectors and the tangent vector $\mathbf{p}_i$, resp. $\mathbf{p}_j$, to the centreline of the fibre

i, resp. j, it was possible to calculate $l_i = \| \mathbf{AB} \times \mathbf{p}_i \|$, resp. $l_j = \| \mathbf{CD} \times \mathbf{p}_j \|$, and finally to obtain the bond surface S between two contacting fibres as follows:

$$S = \frac{l_i l_j}{\|\boldsymbol{p}_i \times \boldsymbol{p}_j\|}. \quad [3]$$

Practically, it was possible to assess the surface of about 80 bonds per specimen to build bond area surface distribution functions. The interval size for plotting frequency distributions is set to 5 μm for Δs and to 50 μm^2 for S.

• *Characterisation of the bonding degree ratio between fibres* – For each bond i along a given fibre, the ratio l_i/L between the bond width l_i and the fibre width L was calculated. This measure can be considered as assessing the "degree" of bonding: a ratio of 1 stands for a full contact and a lower ratio stands for a partial contact for the studied fibre. Here the interval size for plotting frequency distributions is set to 5%.

Results

Influence of the wet pressing on the fibre cross section geometry and inclination

Fig 6(a) shows the fibre width distribution for two pressing conditions. It clearly appears that the fibre width distribution is shifted towards higher values for the high pressing of 0.51 MPa compared to the low pressing of 0.10 MPa. This is also illustrated by the calculated mean width values presented in *Table 2* which increase from 18% between the two packing stresses. A slightly larger standard deviation of the width distribution σ_L is also observed in *Table 2* for the high pressing compared to the low pressing showing that such operation induces a more pronounced heterogeneity of this geometrical property.

This results in ratios of the standard deviation of the width to the mean width $\langle L \rangle$ which are quite similar in both pressing conditions (see *Table 2*). Thus, the heterogeneity of the fibre width in those papers does not appear to be importantly affected by the wet pressing.

Fig 6(b) illustrates that there is no clear difference on the distribution of the thickness l_1 of the fibre cross sections induced by the pressing on this parameter, which is confirmed by the mean values $\langle l_1 \rangle$ and the standard deviations σ_{l1}, as well as by the ratio of these two latter parameters given in *Table 2*. However, the packing stress tends to decrease the thickness l_2 of the fibres as revealed in *Fig 6(c)* and in *Table 2*. A diminution of 34% of the mean values of this thickness parameter is observed between the low and high pressing conditions. The ratios of the standard deviation σ_{l2} to the mean value $\langle l_2 \rangle$ is also much greater in the low pressing case than in the strong pressing case, thus showing a decrease of the heterogeneity of this geometrical property.

The evolutions of the three previous geometrical parameters show the morphological changes of the fibre cross sections occurring during wet pressing. In all pressing conditions, the fibre cross sections were uncollapsed (open lumen), partially or fully collapsed. This is shown by comparing the width L with l_1 or l_2. L is mainly greater than l_1 or l_2. Visually, fibres of papers that were low pressed did not exhibit a dominant cross section shape:

Table 2. Mean width $\langle L \rangle$, thickness $\langle l_1 \rangle$, thickness $\langle l_2 \rangle$, and inclination angle $\langle \theta \rangle$ of fibre cross sections for various pressing conditions, and related standard deviations of such parameters, respectively σ_L, σ_{l1}, σ_{l2} and σ_θ.

Packing stress σ_0 (MPa)	**0.10**	**0.51**
Mean width $\langle L \rangle$ (μm)	30.6	36.1
Standard deviation σ_L (μm)	8.6	9.8
$\sigma_L/\langle L \rangle$	28%	27%
Mean thickness $\langle l_1 \rangle$ (μm)	6.8	6.3
Standard deviation σ_{l1} (μm)	2.0	1.8
$\sigma_{l1}/\langle l_1 \rangle$	29%	29%
Mean thickness $\langle l_2 \rangle$ (μm)	6.1	4.5
Standard deviation σ_{l2} (μm)	2.4	1.3
$\sigma_{l2}/\langle l_2 \rangle$	39%	29%
Mean inclination angle $\langle \theta \rangle$ (°)	-1.76	0.02
Standard deviation σ_θ (°)	23.4	14.1

uncollapsed, partially or fully collapsed cross sections were present. In the case of papers that were more pressed, the fibre cross sections appeared more often fully collapsed.

This corroborates the measured evolution for the ratios of the standard deviation to the mean value of l_2 between the two pressing conditions. Thus, the greater the packing stress the more the shapes of the cross sections of the fibres are homogenised and the more the cross sections collapse at their centres. The relatively low change of l_1 could be related to a limited change of the curvature of the fibre cross sections at their extremities.

Fig 6(d) shows the distribution of the inclination angle θ between the major axis of the fibre section and the plane of the sheet. It shows that the major axis is mostly parallel to the plane of the sheet. The mean values $\langle \theta \rangle$ for both pressing conditions are not equal to zero (see *Fig 6(d)* and *Table 2*). This might be due to an inclination of the main plane of the paper specimen with respect to the X-ray microtomography ($\mathbf{e}_1$, $\mathbf{e}_2$) frame that was very limited. More interestingly, note that the angle distributions shown in *Fig 6(d)* for both pressing conditions are quite symmetric with respect to the mean values of θ. This shows that there is no preferred inclination of the fibre cross sections in such paper specimens. However, the peak of the distribution is higher in the case of the high pressing compared to the low pressing (see also the diminution of the standard deviation of θ in *Table 2*). The packing stress σ_0 thus tends to reduce the inclination angle of the fibre cross sections the main axes of which being more parallel to the main plane of the specimens when increasing the wet pressing.

Influence of the wet pressing on the distance between fibre-fibre bonds and the bond area surfaces

In *Fig 7a,* the distribution functions of the distance Δs between the centers of fibre-fibre bonds are plotted for the two investigated wet pressing conditions. The mean value $\langle \Delta s \rangle$ of the distributions is lower in the case of the highest pressing compared to the lowest, as shown in *Table 3*. However, the largest ratio of the standard deviation $\sigma_{\Delta s}$ to the mean value $\langle \Delta s \rangle$ is obtained in the

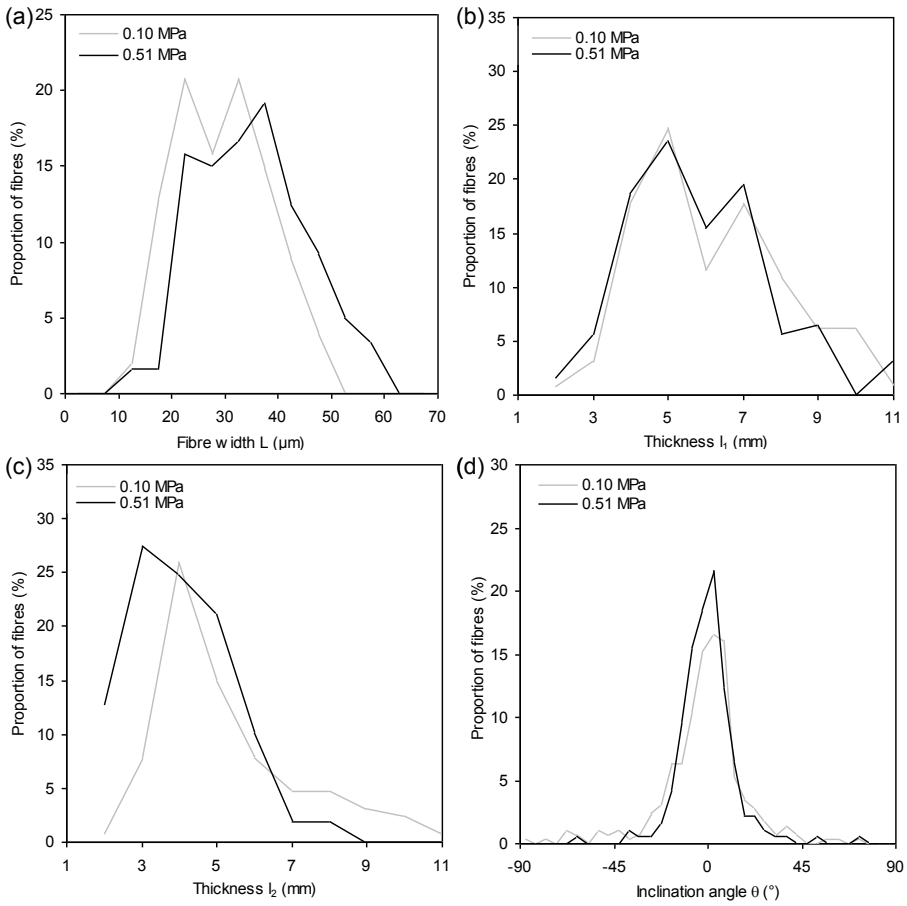

Fig 6. Distributions of the fibre (a) width L, (b) thickness l_1, (c) thickness l_2, and (d) distribution of the inclination angle θ of the fibre cross sections for two pressing conditions.

case of the highest pressing showing an increased heterogeneity of this property due to wet pressing. Two possible changes in the microstructure can be at the origin of such evolution: the change in the inclination angle of the fibre cross sections (see *Table 3*) and the increase of the number of fibre-fibre bonds both induced by wet pressing.

The distributions of the bonding degree ratio l_i/L are plotted in *Fig 7(b)* for both studied wet pressing conditions. Both distributions have quite similar shapes, except for l_i/L values ranging between 0% and 20%. In this range, it appears that there are a lot of bonds having a low bonding degree ratio for the lowest pressing at 0.10 MPa, whereas such types bonds are drastically diminished for the highest wet pressing at 0.51 MPa. Furthermore, the proportion of bonds with $l_i/L > 20\%$ is higher for the pressing at 0.51 MPa compared to that at 0.10 MPa. The bonding degree ratio increase between these two pressing conditions is also underlined by the increase of 20% of the mean value of the bonding degree ratio l_i/L (see *Table 3*) between the low and high pressing conditions. Such increase of the bonding degree ratio corresponds to a respective gain of 42% of the bond width l_i. However, it is obvious that the major part of the bonds is partial for both pressing conditions. Finally, as the ratio of the standard deviation $\sigma_{li/L}$ to the mean value of the bonding degree ratio $\langle l_i/L \rangle$ is diminished when increasing the pressing, the bonds have a tendency to get more geometrical homogenised properties with the wet pressing.

The distributions of the bond area surface are displayed in *Fig 7(c)* for the two pressing conditions. The bond area surface ranges between ≈ 10 to ≈ 1500 µm^2 for both pressing conditions. A larger amount of bonds having a low surface (S < 250 µm^2) is present in the low pressed paper compared to the high pressed paper. The increase of the bond area surface while increasing the wet pressing is also observable when considering the mean bond area surfaces $\langle S \rangle$ displayed in *Table 3* and equal to 337 µm^2 and to 380 µm^2, for the low and high pressings, respectively. Thus, there is a growth of 13% of the mean value of the bond area surface due to the increased packing stress during wet pressing.

Table 3. Mean distance between the centres of two consecutive bonds $\langle \Delta s \rangle$, ratio between bonded width and fibre width $\langle l_i/L \rangle$ and surface of bonds $\langle S \rangle$ for various pressing conditions, and related standard deviations of such parameters, respectively $\sigma_{\Delta s}$, $\sigma_{li/L}$ and σ_S.

Packing stress σ_0 (MPa)	**0.10**	**0.51**
Mean inter bond distance $\langle \Delta s \rangle$ (µm)	35.9	32.4
Standard deviation $\sigma_{\Delta s}$ (µm)	16.5	24.5
$\sigma_{\Delta s}/\langle \Delta s \rangle$	46%	76%
Mean bonding degree ratio $\langle l_i/L \rangle$ (%)	30	36
Standard deviation $\sigma_{li/L}$ (µm)	25	25
$\sigma_{li/L}/\langle l_i/L \rangle$	83%	69%
Mean bond area surface $\langle S \rangle$ (µm^2)	337	380
Standard deviation σ_S (µm^2)	374	400
$\sigma_S/\langle S \rangle$	111%	105%

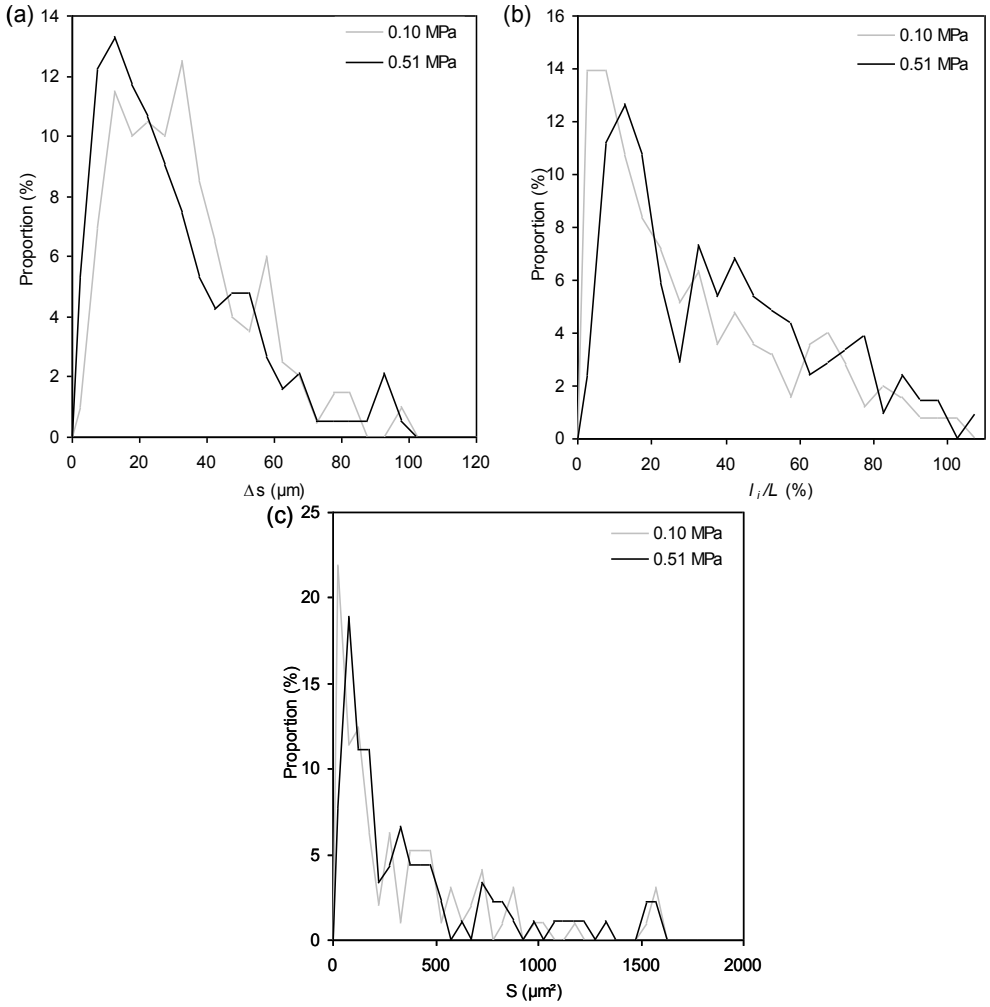

Fig 7. Distributions of (a) the distance Δ*s* between centres of bonds, (b) the bonding degree ratio l_i/L, and (c) the bond area surface *S* for both wet pressing conditions.

However, as exemplified by the values of the ratios $\langle S \rangle / \sigma_S$ in *Table 3*, the heterogeneity of the bond area surface is slightly decreased with the increase of wet pressing. Similarly to the previous observation for l_i/L, the wet pressing can be considered as homogenising the bonds' geometry of the paper.

Discussion

Several microscopy techniques were developed to observe the morphological features of fibres and bonds. They were devoted to the analysis of fibres and bonds present in paper fibrous networks (He et al. 2003a; He et al. 2003b; He et al. 2004; Batchelor 2006; Chinga-Carrasco 2010; Wiltsche 2011) or of fibres and bonds that were especially and individually prepared (Thomson 2007; Thomson 2008a; Thomson 2008b; Kappel 2009; Kappel 2010). For instance, He et al. (He et al. 2003a; He 2003b; He et al. 2004; Batchelor et al. 2006a) applied confocal laser scanning microscopy to study the morphology of fibres and to determine the number of bonds and their inter bond distance in paper handsheets. This technique utilises specimens where fibres are first dyed (He et al. 2003a) and then embedded in an epoxy resin. Such assembly is then ground to expose the specimen cross-sections. It is therefore a destructive technique that requires a careful preparation of the studied specimens. Furthermore, it seems that the serial grinding can only be performed in an arbitrary direction that may cause some difficulties to perform a complete 3D analysis of the geometry of all fibres and inter bond distances. Compared to the microscopy techniques, X-ray microtomography obviously allows such versatility when investigating 3D structures to obtain quantitative microstructural data. However, the approach of He et al. allows the measurement of geometrical parameters for a reasonably large set of individual fibres in a network. The technique was applied to highlight morphological changes induced by wet pressing and delivered noticeable data. The comparison and the similarity of their observations with ours are addressed below.

Recently, Kappel et al. (2009; 2010) used polarised light microscopy to visualize individual fibre-fibre bonds. In Kappel et al. (2009), they compared their results to cross-sectional microtome sectioning technique, see another example of such microtome technique in Wiltsche et al. (2011), combined to image analysis. Thomson et al. (2007) used fluorescence microscopy to observe fibre-fibre bonds, the effect of drying and rewetting (Thomson et al. 2008a), or pressing (Thomson et al. 2008b) on bonds. These three techniques (polarized light microscopy, fluorescence microscopy and cross-sectional microtome sectional and image analysis) allow few

measures to be performed on single fibre-fibre bonds that are extracted from extremely low basis weight handsheets (Thomson et al. 2008b; Kappel et al. 2009). Therefore the network influence on the development of their morphology during papermaking unit operations may be lost; cf. conclusion remark in Kappel et al. (2009). This appears as a main drawback despite the precision of their dimensional measurements. The average surface of bonds that was determined by some of these authors (for example, 1130 μm^2 for mixed spruce and pine kraft pulp fibres in Kappel et al. (2009)) is quite larger than the present measured average bond surface (average bonds' surface ranging between 337 and 380 μm^2; see *Table 3*) for fibres having in all cases cross-section dimensions that may be reasonably comparable. Even though the surface of the bonds that are measured by the microtomography approach or by the microscopic approaches are of the same order, their average values exhibit a great difference that might reflect the influence of the bond preparation technique. Moreover, such comparisons are extremely delicate to carry out as all fibres used in the literature work may have been extracted or treated differently. Further work has to be performed to complete the quantitative database on the bond morphology and surface using X-ray microtomography, but also using the various recently improved microscopy techniques.

The various microstructural descriptors that have been defined and measured in this study are not exhaustive. However, they deliver important information about both the mechanisms of the changes of pulp fibre networks, and of the morphology of fibre cross sections and bonds induced by the wet pressing operation. The fibre cross section inclination, width and thicknesses could have been determined. In parallel, an unprecedented in situ analysis of the fibre-fibre bond surface in pulp fibre networks could have been undertaken with some highlights on the bond area surface and on the so-called relative bonding degree.

Some trends associated to the consolidation of the paper fibrous network during wet pressing are clearly highlighted:

• At low pressing, the fibre cross sections and bonds exhibit quite heterogeneous morphological properties. The heterogeneity of the measured structural data was generally reduced when increasing the wet pressing, except the distance between bonds which quite astonishingly increased.

• The analysis of the changes of the cross sections of the fibres, i.e. the transverse changes of fibres, during wet pressing reveals several features: for example, at low pressing the cross sections of fibres are predominantly uncollapsed or partially collapsed, and exhibit a large variety of inclination angles. At high pressing, the cross sections of fibres tend to fully collapse, and their inclination is reduced: their major axis becomes parallel to the main plane of paper sheets.

• Further, the bonding degree ratio is low at low pressing and increases at high pressing. The bond surfaces follow on the average a similar trend. The mechanisms of such increases might be related to the collapse of the fibre cross sections and to the change of their inclination angles.

The validity of the observations performed using the X-ray images is supported by the similitude of the measured distributions for some parameters that are common to our study and in studies by He et al. (He et al. 2003b; He et al. 2004) for the paper behaviour during wet pressing. For instance, the distributions measured for Δs, which is the so-called free segment lengths defined by He et al., show a great similitude in their shapes. The peak values of the histograms are close in both approaches and follow the same trend: i.e. a shift of the peak values towards lower inter-bond distances as the wet pressing increases (He et al. 2004). Likewise some observations we made regarding the changes of the cross section inclination angles compared with the main plane of the paper sheet resemble the previous observations of these authors (He et al. 2003b). In both cases, the peaks of the distributions are located at 0° and their values are similar. The distributions become also narrower as the wet pressing increases. Finally, the improvement of the homogeneity of the microstructure properties related to fibres and bonds is also apparent in the results by He et al. (2003b; 2004).

Briefly speaking, some of the previous quantitative data about the microstructure of fibres and bonds could be useful to create realistic fibre network models or to enrich the existing approaches for the prediction of the mechanical behaviour of paper: e.g. for describing the evolution of parameters such as the Young's modulus and the breaking strain as displayed in *Fig 4*.

The observed increase of these macroscopic mechanical properties with the wet pressing increase is obviously related to the individual morphological and mechanical properties of fibres and bonds, and also to the number of these latter. The previous experimental analysis provides a lot of useful morphological data to explain the observed trends: for instance the collapse and the alignment of the fibre cross-sections in the plane of the paper sheet induce (i) an increase of the bond degree ratio, (ii) an increase of the bond surface and (iii) a diminishing of the distance between the centre of bonds (or an increase of the number of bonds per fibre). From these changes, it can be inferred, for example, that the mechanical properties of the bonds and of the inter bond fibre segments will be improved and so the network properties.

Furthermore, some existing models (Jayaraman, Kortschot 1998) take into account the surface of bonds between fibres and the fibre cross section by introducing the so-called Relative Bonded Area (RBA), i.e. the fraction of fibre surface in contact with other fibres (Niskanen, Rajatora 2002; Sampson 2004). The above experiments show that it would be possible to take into account in mechanical models a description of the bond surface which would be statistically finer. This argument holds also for more recent network models where the bond description remains unfortunately quite poor due to the lack of reliable experimental geometric data.

Conclusion

The X-ray microtomography technique allows a 3D and discrete analysis of the morphology of individual fibres and bonds of fibre networks to be carried out. The efficiency of the technique was illustrated to analyse fibre and bond geometry changes induced by wet pressing in paper sheets. It was established that an increase of wet pressing had a general tendency to homogenise the geometrical properties of fibre cross sections and bonds. Furthermore, such increase makes the fibre cross sections collapse and their inclination change. At low wet pressing, most bonds are partial and their surfaces are limited, whereas the bonding "degree" ratios and the bond surfaces are increased at higher pressing. Such results were compared with those obtained in the literature by serial cross section grinding and microscopy. They display a good agreement with the previous observations. But they also improve them, particularly regarding the bond surface analysis. It is noticeable that the mean surface of bonds in fibrous networks might appear as being largely lower compared to that measured using single fibre-fibre bonds. The potential of X-ray measurements to profit network models for the prediction of the mechanical behaviour of papers was also briefly discussed.

Acknowledgements

This work was performed within the ESRF Long Term Project "Heterogeneous Fibrous Materials" (exp. MA-127) and the ANR research program "3D discrete analysis of deformation micro-mechanisms in highly concentrated fiber suspensions" (ANAFIB, ANR-09-JCJC-0030-01). C. Marulier would like to thank the Région Rhône-Alpes (France) for his research grant.

Literature

S.D. Alexander, R. Marton (1968): Effect of beating and wet pressing on fiber and sheet properties, Tappi, 51(6), 283-288.

C. Antoine, P. Nygard, O. Weiby Gregersen, R. Holmstad, T. Weitkamp, C. Rau (2002): Binarisation of 3d images of paper obtained by phase-contrast X-ray microtomography, Nucl. Instr. and Meth. A490, 392-402.

P.A. Åslund, P. Isaksson (2011): A note on the nonlinear mechanical behaviour of planar random network structures subjected to in-plane compression, J. Compos. Mat., 45(25), 2697-2703.

M. Axelsson, S. Svensson (2010): 3D pore structure characterisation of paper, Pattern Anal. Applic., 13, 159-172.

J. Baruchel, E. Boller, P. Cloetens, W. Ludwig, F. Peyrin (2000): Microtomography at a third generation synchrotron radiation Facility In "X-Ray Tomography in Material Science", ed. Baruchel, Buffière, Maire, Merle, Peix, Ed. Hermes (Paris), 45-59.

W.J. Batchelor, R.P. Kibblewhite (2006a): Calculation of relative bonded area and scattering coefficient from sheet density and fibre shape, Holzforschung, 60(3), 253-256.

W.J. Batchelor, J. He, W.W. Sampson (2006b): Inter-fibre contacts in random fibrous materials: experimental verification of theoretical dependence on porosity and fibre width, J. Mater. Sci., 41(24), 8377-8381.

G. Chinga, O. Solheim, K. Mörseburg (2007): Cross-sectional dimensions of fiber and pore networks based on Euclidean distance maps, Nord. Pulp Pap. Res. J., 22(4), 500-507.

G. Chinga-Carrasco, P.O. Johnsen, K. Øyaas (2010): Structural quantification of wood fibre surfaces - Morphological effects of pulping and enzymatic treatment, Micron, 41, 648-659.

G. Chinga-Carrasco (2011): Microscopy and computerized image analysis of wood pulp fibres multiscale structures, Microscopy: Science, Technology, Applications and Education, edited by Méndez-Vilas A. and Díaz J., 2182-2189.

C. Délisée, E. Badel, J. Lux, J. Malvestio (2009): 3D microstructural characterization and local densification of cellulosic fibrous insulators under compression, Eur. J. Env. Civ. Eng., 13(4), 429-442.

O. Guiraud, L. Orgéas, P.J.J. Dumont, S. Rolland du Roscoat (2012): Microstructure and deformation micro-mechanisms of concentrated fiber bundle suspensions: an analysis combining X-ray microtomography and pull-out tests, J. Rheol.,56, 593-623.

J. He, W.J. Batchelor, R. Markowski, R.E. Johnston (2003a): A new approach for quantitative analysis of paper structure at the fibre level, Appita J., 56(5), 366-370.

J. He, W.J. Batchelor, R.E. Johnston (2003b): The behavior of fibers in wet pressing, Tappi J., 2(12), 27-31.

J. He, W.J. Batchelor, R.E. Johnston (2004) A microscopic study of fibre-fibre contacts in paper, Appita J., 57(4), 292-298.

S. Heyden, P.J. Gustafsson (2001): Stress-strain performance of paper and fluff by network modelling, 12th Fundamental Research Symposium, Oxford.

R. Holmstad, A. Goel, S. Ramaswamy, O.W. Gregersen (2006): Visualization and characterization of high resolution 3D images of paper samples, Appita J., 59(5), 370-377.

K. Jayaraman, M.T. Kortschot (1998): Closed-form networks models for the tensile strength of paper - a critical discussion, Nord. Pulp Pap. Res. J., 13(3), 233-242.

L. Kappel, U. Hirn, W. Bauer, R. Schennach (2009): A novel method for the determination of bonded area of individual fibre-fibre bonds, Nord. Pulp Pap. Res. J., 24(2), 199-205.

L. Kappel, U. Hirn, E. Gilli, W. Bauer, R. Schennach (2010a): Revisiting polarized light microscopy for fiber-fiber bond area measurement - Part I: Theoretical fundamentals, Nord. Pulp Pap. Res. J., 25(1), 65-70.

L. Kappel, U. Hirn, E. Gilli, W. Bauer, R. Schennach (2010b): Revisiting polarized light microscopy for fiber-fiber bond area measurement - Part II: Proving the applicability, Nord. Pulp Pap. Res. J., 25(1), 71-75.

V. Koivu, M. Decain, C. Geindreau, K. Mattila, J.-F. Bloch, M. Kataja (2009): Transport properties of heterogeneous materials. Combining computerised X-ray micro-tomography and direct numerical simulations, Int. J. Comput. Fluid D., 23(10), 713-721.

V. Koivu, R. Seppänen, T. Turpeinen, K. Mattila, J. Hyväluoma, M. Kataja (2010): Combining X-ray micro-tomography and image analysis to study imbibition and void space in liquid packaging board, J. Pulp Pap. Sci., 36(3-4), 170-179.

P. Latil, L. Orgéas, C. Geindreau, P.J.J. Dumont, S. Rolland du Roscoat (2011): Towards the 3D in situ characterisation of deformation micro-mechanisms within a compressed bundle of fibres, Comp. Sci. Technol., 71, 480-488.

T.-H. Le, P.J.J. Dumont, L. Orgéas, D. Favier, L. Salvo, E. Boller (2008): X-Ray Phase Contrast Microtomography for the Analysis of the Fibrous Microstructure of SMC Composites, Compos. Part A-Appl. S., 39, 91-103.

J.X. Liu, Z.T. Chen, H. Wang, K.C. Li (2011): Elasto-plastic analysis of influences of bond deformability on the mechanical behavior of fiber networks, Theor. Appl. Fract. Mec., 55, 131-139.

P. Luner, A.E.U Kärnä , C.P. Donofrio (1961): Studies in interfibre bonding of paper. The use of optical bonded area with high yield pulps, TAPPI J., 44(6), 409-414.

F. Malmberg, J. Lindblad, C. Ostlund, K.M. Almgren, E.K. Gamstedt (2011): Measurement of fibre-fibre contact in three-dimensional images of fibrous materials obtained from X-ray synchrotron microtomography, Nucl. Instrum. Methods, 637, 143-148.

H. Nanko, J. Ohsawa (1989): Mechanisms of fibre bond formation, Fundamentals of Papermaking, Trans. IXth Fund. Res. Symp. Cambridge.

K. Niskanen, H. Rajatora (2002) Statistical geometry of paper cross-sections, J. Pulp Pap. Sci., 28(7), 228-233.

L. Orgéas, P.J.J. Dumont, J.-P. Vassal, O. Guiraud, V. Michaud, D. Favier (2012): In-plane conduction of polymer composite plates reinforced with architectured networks of Copper fibres, J. Mat. Sci., 47, 2932-2942.

P. Perona, J. Malik (1990): Scale space and edge detection using anisotropic diffusion, IEEE T. Pattern Anal., 12, 629-639.

S. Rolland du Roscoat, X. Thibault, J.-F. Bloch (2005): Synchrotron radiation microtomography applied to investigation of paper, J. Phys. D Appl. Phys., 38, A78-A84.

S. Rolland du Roscoat, M. Decain, X. Thibault, C. Geindreau, J.-F. Bloch (2007): Estimation of microstructural properties from synchrotron X-ray microtomography and determination of the REV in paper materials, Acta Mater., 55, 2841-2850.

S. Rolland du Roscoat, M. Decain, C. Geindreau, X. Thibault, J.-F. Bloch (2008): Microstructural analysis of paper using synchrotron X-ray microtomography: numerical estimation of the permeability and effective thermal conductivity, Appita J., 61, 286-290.

L. Salmén, C. Fellers (1989): The nature of volume hygroexpansivity of paper, J. Pulp Paper Sci., 15(2), 63-65.

L. Salvo, M. Suéry, A. Marmottant, N. Limodin, D. Bernard (2010): 3D imaging in material science: Application of X-ray tomography, C.R. Phys., 11, 9-10.

E. J. Samuelsen, E. J., Helle, T., Houen, P. J., Gregersen, O. W., Raven, C. (1999): Three-dimensional imaging of paper by use of Synchrotron X-Ray Microtomography, International Paper Physics Conference, 307-312.

E. J. Samuelsen, P. J. Houen, O. W. Gregersen, T. Helle, C. Raven, (2001): Three-dimensional imaging of paper by use of synchrotron x-ray microtomography, J. Pulp Pap. Sci., 27(2), 50-53.

W.W. Sampson (2004): A model for fibre contact in planar random fibre networks, J. Mat. Sci. 39, 2775-2781.

W.W. Sampson (2009): Materials properties of papers as influenced by its fibrous microstructure, Int. Mater. Rev., 54(3), 134-156.

J. Strömbro, P. Gudmundson (2008): An anisotropic fibre-network model for mechano-sorptive creep in paper, Int J Solids Struct., 45, 5765-5787.

C.I. Thomson, R.M. Lowe, A.J. Ragauskas (2007): Imaging celulose fibre interfaces with fluorescence microscopy and resonance energy transfer, Carbohyd. Polym., 69(4), 799-804.

C.I. Thomson, R.M. Lowe, A.J. Ragauskas (2008a): First characterization of the development of bleached kratf softwood pulp fiber interfaces during drying and rewetting using FRET technology, Holzforschung, 62, 383-388.

C. Thomson, R. Lowe, D. Page, A. Ragauskas (2008b): Exploring fibre-fibre interfaces via FRET and fluorescence microscopy, J. Pulp Pap. Sci., 34(2), 113-119.

A. Torgnysdotter, A. Kulachenko, P. Gradin, L. Wågberg (2007): The link between the fiber contact zone and the physical properties of paper: a way to control paper properties, J. Compos. Mat., 41(13), 1619-1633.

T. Uesaka, C. Moss, Y. Nanri (1991): The characterization of hygroexpansivity in paper, International Paper Physics Conference Proceedings, TAPPI Press, Atlanta (GA), USA, 613-622.

P. Vernhes, A. Blayo, J. F. Bloch, B. Pineaux (2007): A new approach to model and characterize the heating up and spreading of toner particles trough the nip of an electrophotographic printer, Taga J., 3, 188-203.

J. Viguié, P.J.J. Dumont, E. Mauret, S. Rolland du Roscoat, P. Vacher, I. Desloges, J.-F. Bloch (2011): Analysis of the hygroexpansion of a lignocellulosic fibrous material by digital correlation of images obtained by X-ray synchrotron microtomography: application to a folding box board, J. Mat. Sci., 46(14), 4756-4769.

M. Wiltsche, M. Donoser, J. Kritzinger, W. Bauer (2011): Automated serial sectioning applied to 3D paper structure analysis, J. Microsc., 242, 197- 205.